

Supporting Information

**Fluorinated Carbon Encapsulated NiO Cluster/TiO₂ Nanotubes as a Robust
Photocatalyst for Hydrogen Evolution**

Lihong Yuan,^{a,‡} Panpan Wang,^{b,‡} Chunyao Niu,^{b,‡} Chenghua Sun,^c Rachel A. Caruso^d and Xiao Li

Zhang^{a,*}

^a*School of Materials Science and Engineering, Zhengzhou University, 450001 P.R. China.*

^b*School of Physics and Microelectronics, Zhengzhou University, 450001 P.R. China.*

^c*Faculty of Science, Engineering & Technology, Swinburne University of Technology, VIC 3122, Australia.*

^d*Applied Chemistry and Environmental Science, School of Science, RMIT University, Melbourne, VIC 3001, Australia.*

[‡]*Equal contribution from L. Yuan, P. Wang and C. Niu.*

^{*}*Corresponding author. E-mail: xiaolizhang.z@gmail.com.*

Experimental Details

Chemicals

The material syntheses used reagent grade chemicals including sodium hydroxide, ethanol, nickel nitrate hexahydrate (98%), hydrochloric acid (37%), glucose (98%), ammonium fluoride, methanol and Nafion (5.0 wt.%) from Sinopharm Chemical Reagent Co., Ltd (Shanghai, China), and Degussa P25 TiO₂ nanoparticles from Evonik. Milli-Q water (resistivity of 18.2 mΩ·cm) was used throughout this work.

Materials synthesis

Synthesis of NiO cluster/TiO₂ nanotubes (NT-x): After dispersing P25 TiO₂ particles (1.0 g) in 60 mL of 5 M sodium hydroxide solution under magnetic stirring, the white slurry was transferred into a 100 mL Teflon-lined stainless-steel autoclave for hydrothermal reaction at 140 °C for 10 h. The product was rinsed with water for three times to remove residual sodium hydroxide before being collected by centrifugation and redispersed into 0.1 M hydrochloric acid aqueous solution (1000 mL) under moderate stirring to obtain hydrogen titanate. Rinsing thoroughly with water for three times, the hydrogen titanate was collected by centrifugation then redispersed into a nickel nitrate aqueous solution (80 mL) under magnetic stirring to give an expected Ni/Ti weight percentage of 0.5, 1.0, 2.0, 3.0 or 5.0wt%. After washing with water and then ethanol, each three times, the samples were dried under vacuum at room temperature overnight before being calcined in a muffle furnace at 450 °C for 2 h in air using a ramp rate of 2 °C/min from room temperature (ca. 20 °C) to obtain NiO cluster/TiO₂ nanotubes (NT-x). The x in the NT-x nomenclature corresponds to the Ni-loading during the synthesis, resulting in samples labelled NT-0.5, NT-1, NT-2, NT-3 and NT-5. TiO₂ nanotubes were also obtained following calcination of the hydrogen titanate in the absence of the NiO deposition step. R-NT-1 and

R-FNT-1 denotes the retrieved NT-1 and FNT-1 composite after 3 h HER reaction, respectively.

Preparation of carbon encapsulated NT-1 (CNT-y): NT-1 (0.2 g) was ultrasonically dispersed into 60 mL glucose aqueous solution to give an expected weight C/Ni percentage of 0.5, 1.0 and 2.0 wt%, before hydrothermal reaction in the 100 mL Teflon-lined stainless-steel autoclave at 150 °C for 15 h. The products were collected after washing with deionized water and then ethanol each three times and dried at 60 °C for 6 h, and labelled as CNT-0.5, CNT-1 and CNT-2.

Preparation of fluorinated carbon encapsulated NT-x (FNT-x): The FNT-x catalysts were synthesized through the same procedure as the carbon encapsulation in an aqueous solution containing glucose and ammonia fluoride in an expected weight F/C/Ni percentage of 1/2/2. The resulting samples were labelled as FNT-0.5, FNT-1, FNT-2, FNT-3 and FNT-5, corresponding to the nickel oxide loadings used during the syntheses of NT-x.

Preparation of control samples - NiO nanoparticles (NP) and NiO NP/TiO₂ nanotubes: Nickel nitrate (0.15 g) was dissolved in 30 mL deionized water before adding 0.04 g sodium hydroxide under magnetic agitation. The obtained blue colour solution was heated in a water bath at 80 °C until a green precipitate was formed. The precipitate was collected and washed with water and then ethanol each three times, then dried at room temperature overnight before being calcined in a muffle furnace at 450 °C for 2 h in air using a ramp rate of 2 °C/min from room temperature to obtain the control sample of NiO nanoparticles. NiO nanoparticle decorated TiO₂ nanotubes were prepared by dispersing TiO₂ nanotubes into the 30 mL nickel nitrate solution before adding sodium hydroxide using the same Ni/Ti ratio during the preparation of NT-1.

Characterization

A ThermoFisher spherical aberration corrected Spectra 300S/TEM Scanning/Transmission

Electron Microscope (S/TEM) was used to investigate the morphology and conduct elemental mapping of the samples. X-ray diffraction (XRD) patterns obtained on an X-ray diffractometer (Ultima IV) using Cu K α irradiation under a 40 kV working voltage were used to determine the phase of the obtained samples. Raman spectra were acquired on a HORIBA Lab-RAM HR-Evolution Raman spectrometer with laser excitation at 532 nm. The UV/Vis diffuse reflectance spectra (UV/Vis DRS) were obtained with a UV/Vis/NIR spectrophotometer (UH4150, Hitachi, Japan) in the wavelength range 300-800 nm. The photoluminescence spectra were recorded on a fluorospectro photometer (F-280-Laser-NIR, Gangdong Science and Technology Development Co., LTD. Tianjin) with an excitation wavelength of 460 nm. X-ray photoemission spectra were collected using a Thermo Escalab 250xi analyzer. Ni 2p Ti 2p and F 1s binding energies were recorded using Al K α (1486.6 eV) as the excitation source and a pass energy of 23.5 eV. The position of the XPS peaks of the corresponding element was referenced to the C1s peak.

Photocatalytic hydrogen generation

Photocatalytic hydrogen evolution experiments were conducted using a vacuum sealed reaction system at room temperature (20 ± 1 °C) controlled by a cooling water system. The photocatalyst powder (10 mg) was dispersed in 50 mL methanol aqueous solution (10 % by volume) by sonication in a Pyrex flask (350 mL) equipped with a water jacket to exclude the thermal effect from illumination. A 300 W Xe lamp (Perfect Light PLS-SXE300D) was used to simulate solar light, illuminating the top quartz window of the reactor. Gas evolution was monitored by an online gas chromatograph (GC-7860, Ar carrier gas).

Apparent quantum efficiency (AQE) measurement

Measurement of AQE followed the same procedure as the photocatalytic HER test under

monochromatic light obtained by using bandpass filters with different wavelengths (365 nm). The light intensity of monochromatic light was measured by a photometer (Perfect Light, PL-MW2000). The AQE can be obtained by the following equation:

$$AQE = \frac{2 \times N_A \times n_{H_2}}{N_{incident}} \times 100\%$$

where N_A and n_{H_2} represents the Avogadro constant ($6.022 \times 10^{23} \text{ mol}^{-1}$) and amount of produced H_2 molecules, respectively. $N_{incident}$ is the number of incident photons, which can be calculated from:

$$N_{incident} = \frac{Pt}{h\nu} = \frac{ISt\lambda}{hc}$$

where P is the light power (W), t is the irradiation time (s), h is the Planck constant ($6.626 \times 10^{-34} \text{ J}\cdot\text{s}$), ν is the frequency of light (Hz), I is the light intensity ($\text{W}\cdot\text{cm}^{-2}$), S is the illuminated area (cm^2), λ is the wavelength of monochromatic light (nm), and c is the speed of light in vacuum ($3 \times 10^8 \text{ m}\cdot\text{s}^{-1}$).

Photoelectrochemical test

All photoelectrochemical tests were conducted using a conventional three-electrode system at 25 °C on an Electrochemical Workstation (CHI 760E). A platinum plate ($1 \times 1 \text{ cm}^2$), a Ag/AgCl electrode (saturated KCl) and films of the sample on a fluorine doped tin oxide (FTO) coated glass plate ($1 \times 1 \text{ cm}^2$) were used as the counter, reference and working electrode, respectively.

The working electrode was prepared as follows. 20 mg of the synthesised sample was dispersed into a solution of 2.0 mL deionized water, 1.0 mL anhydrous ethanol and 0.1 mL Nafion solution by ultrasonic dispersion. A film of the sample was obtained by dropping 0.01 mL solution on the FTO surface ($1 \times 1 \text{ cm}^2$) and drying at 50 °C for 2 h, forming the working electrode.

Computational simulation details

All of the calculations were based on the spin polarized periodic density functional theory (DFT)

and performed by the Vienna Ab-initio Simulation Package (VASP).^{1,2} The Perdew-Burke-Ernzerhof (PBE) was used to describe the exchange correlation energy.³ In order to describe the Coulomb interaction of the system more accurately, the DFT+U method was used, setting the effective U values on the Ni and Ti to 5.3 and 4.2 eV, respectively.⁴⁻⁷ The van der Waals (vdW) interactions were described by using the DFT-D3 method.^{8,9} To avoid interactions between the two periodic units, the vacuum space was set to 20 Å. The energy cutoff of plane wave basis was set to 450 eV. A total energy convergence of 10⁻⁴ eV was used for structural optimization. The Brillouin zone (BZ) was sampled by the Monkhorst–Pack scheme (MP) special k-point grid including the G-point with a grid density of $2\pi \times 0.03\text{Å}^{-1}$.

To determine the structure of the NiO cluster/TiO₂ composites, ab initio molecular dynamics (AIMD) simulation was performed to search for the optimal structure of a NiO cluster on TiO₂ slab. The simulation was performed in the NVT ensemble employing Nosé–Hoover thermostats, and the temperature was set at 450K and the timestep was 2 fs.^{6,10} More than 6 ps AIMD simulation was performed (Fig. S1), and all the simulations reach the equilibrium after ~4 ps. The final structural configuration is then fully optimized when all forces diminish. The NiO (100) surface was modelled with a (2 × 5) four-Ni-layer slab (44 Ni and 44 O atoms). To accommodate NiO cluster, we utilized a p(2 × 4) periodic slab with three TiO₂ layers (48 Ti and 96 O atoms). A (5 × 6) graphene supercell was used to form a heterojunction with the NiO cluster/TiO₂, with a distance of ~3 Å between the graphene and the NiO cluster. In all structures, the atoms in the bottom half were fixed.

The adsorption energy and Gibbs free energy change of hydrogen were calculated by the following formulas:

$$\Delta E_{H^*} = E_{\text{substrate} + H^*} - E_{\text{substrate}} - \frac{1}{2}E_{H_2}$$

$$\Delta G_{H^*} = \Delta E_{H^*} + 0.24$$

where $E_{substrate + H^*}$ and $E_{substrate}$ are the energies of the catalyst with and without H adsorption, respectively. E_{H_2} is the energy of the molecular hydrogen in the gas phase, and 0.24 is the free energy correction, which was proposed by Norskov et al.¹¹

The equation for calculating the work function was defined as :

$$\Phi = E_{vac} - E_F$$

where E_{vac} and E_F are the electrostatic potentials at the vacuum and Fermi levels, respectively.

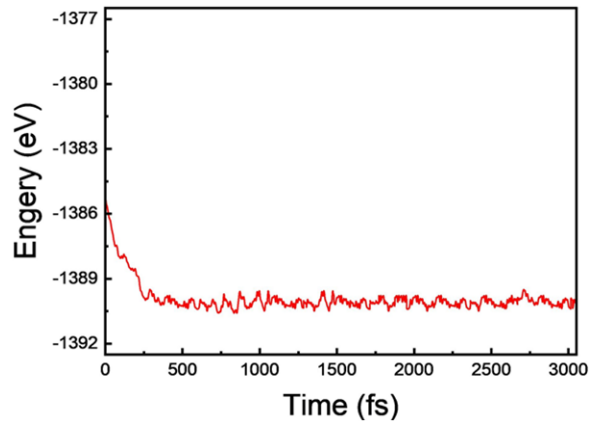


Fig. S1 AIMD simulation trajectories for NiO cluster/TiO₂.

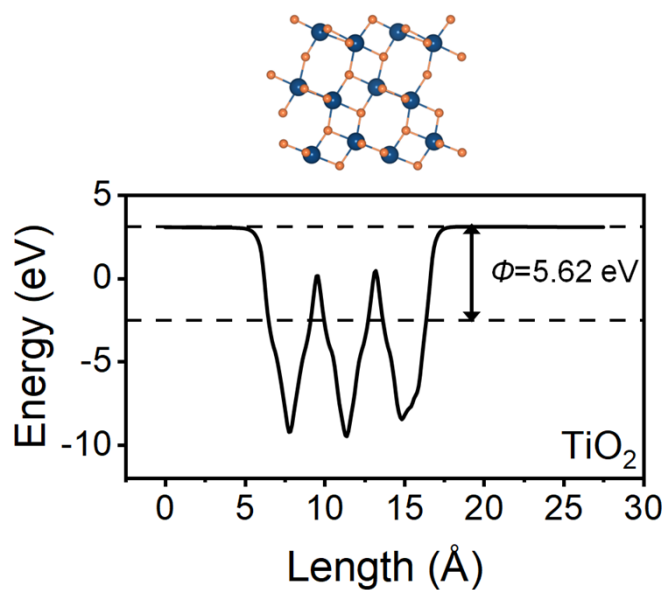


Fig. S2 Structure and work function for TiO_2 (101) surface (Ti, navy blue; O, orange).

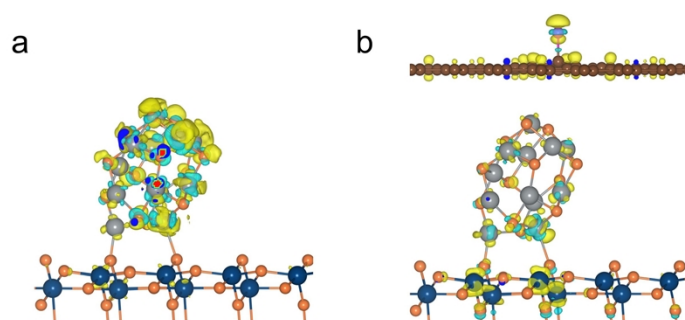


Fig. S3 Photogenerated electron distribution of NiO cluster/ TiO_2 and F-G/NiO cluster/ TiO_2 (Ti, navy blue; O, orange; Ni, gray; yellow and cyan colours represent the accumulation and consumption of charge, respectively; the isosurface value is $0.004 \text{ e}/\text{\AA}^3$).

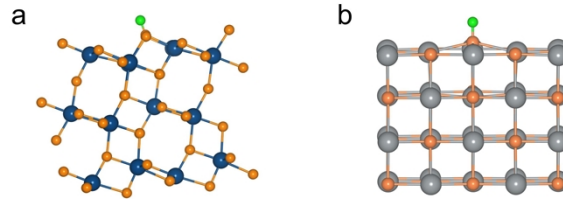


Fig. S4 The position for adsorption of hydrogen on (a) TiO₂ (101) surface and (b) NiO (100) surface (H, green; Ti, navy blue; O, orange; Ni, grey).

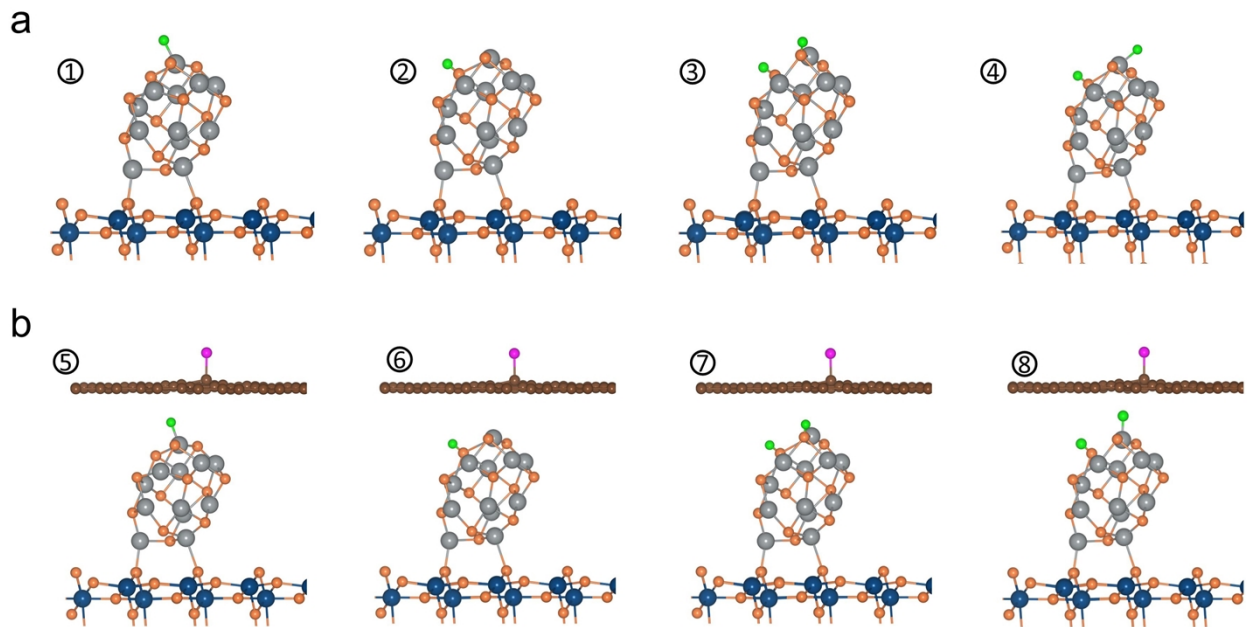


Fig. S5 Optimized structures of hydrogen adsorption on (a) NiO cluster/TiO₂ and (b) F-G/NiO cluster/TiO₂ (H, green; Ti, navy blue; O, orange; Ni, grey). ①, ②, ⑤ and ⑥ are the structures of the first hydrogen adsorption on the Ni and O sites of NiO cluster/TiO₂ and F-G/NiO cluster/TiO₂; ③, ④, ⑦ and ⑧ are the structures of the second hydrogen adsorbed on the Ni and O sites of NiO cluster/TiO₂ and F-G/NiO cluster/TiO₂ with the first hydrogen occupied O site, respectively. The corresponding

adsorption energies ($\Delta E_{H_x^*}$) are listed in Table S2, which is calculated by

$$\Delta E_{H_x^*} = E_{substrate + H_x^*} - E_{substrate + H_{x-1}^*} - \frac{1}{2}E_{H_2},$$

where $E_{substrate + H_x^*}$ and $E_{substrate + H_{x-1}^*}$ are

the adsorption energies of the x th H atom and $(x-1)$ th H atom, respectively. E_{H_2} is the energy of the molecular hydrogen in the gas phase.

Table S1 The adsorption energy of hydrogen on TiO₂, NiO, G/NiO, NiO cluster/TiO₂ and F-G/NiO cluster/TiO₂.

Sample	TiO ₂		NiO		G/NiO		NiO cluster/TiO ₂		F-G/NiO cluster/TiO ₂	
site	O	Ti	O	Ni	O	Ni	O	Ni	O	Ni
ΔE_{H^*} (eV)	0.37	-	0.58	1.14	0.06	1.48	-1.29	0.21	-1.28	0.32

Table S2 The adsorption energy of the first ①, ②, ⑤ and ⑥ or second ③, ④, ⑦ and ⑧ hydrogen on the NiO cluster/TiO₂ and F-G/NiO cluster/TiO₂.

	NiO cluster/TiO ₂				F-G/NiO cluster/TiO ₂			
	①	②	③	④	⑤	⑥	⑦	⑧
ΔE_{H^*} (eV)	0.21	-1.29	-1.21	-0.19	0.32	-1.28	-1.13	-0.30

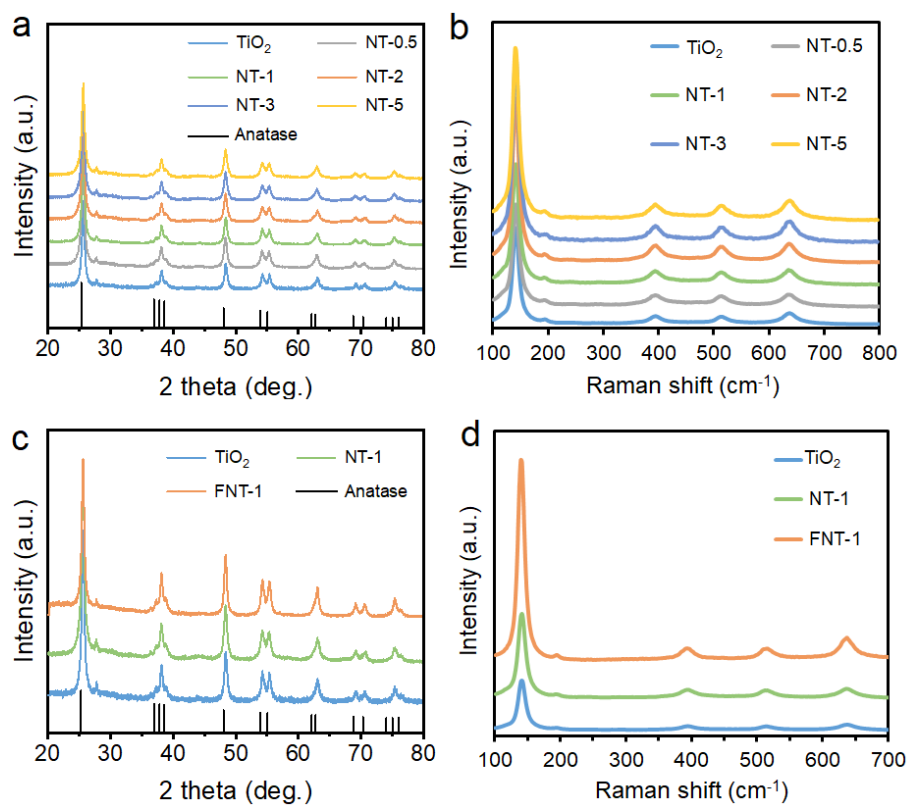


Fig. S6 XRD patterns (a) and Raman spectra (b) of the NT-x. XRD patterns (c) and Raman spectra (d) of the TiO₂ nanotubes (TiO₂), NT-1 and FNT-1.

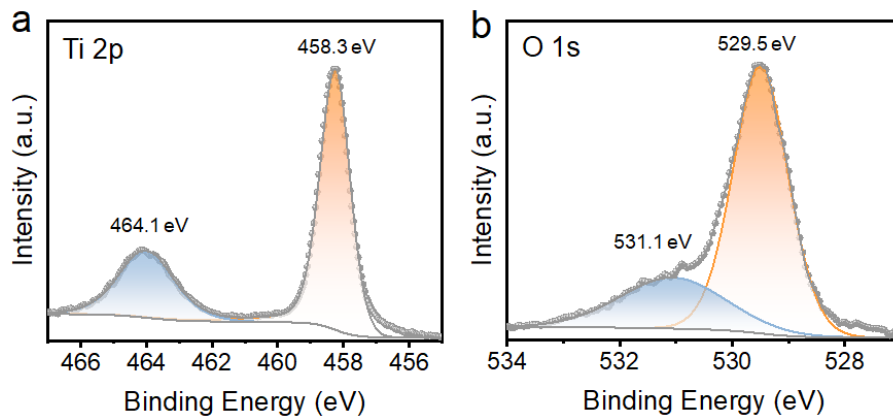


Fig. S7 High-resolution XPS spectra of (a) Ti 2p and (b) O 1s of the TiO₂ nanotubes.

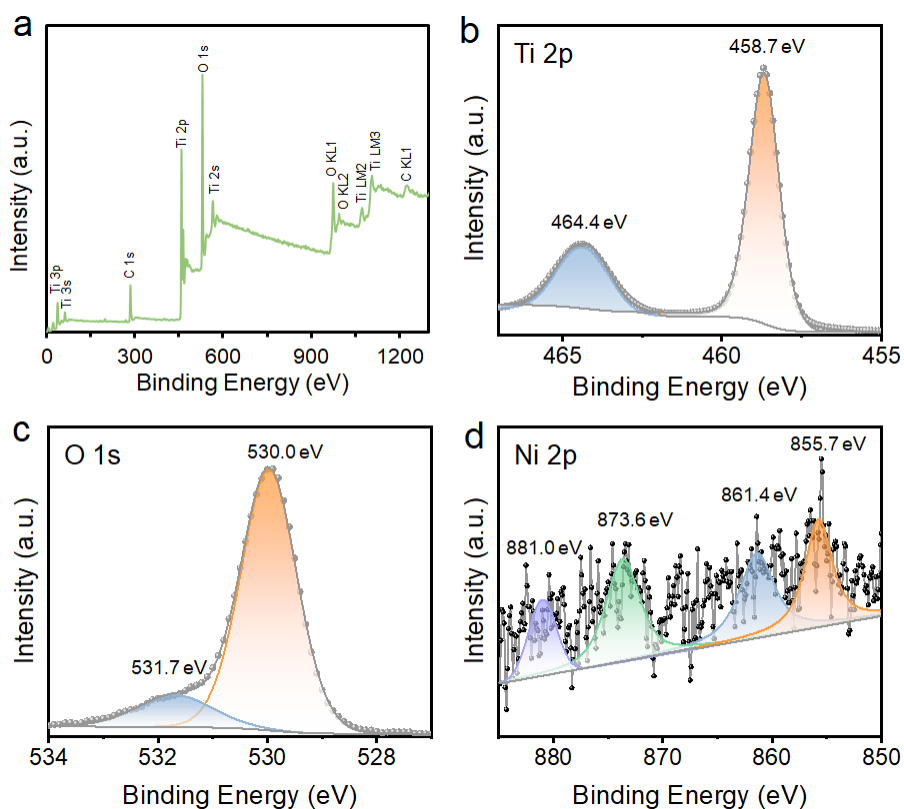


Fig. S8 (a) Overall XPS spectrum and high-resolution XPS spectra of (b) Ti 2p (458.7 and 464.5 eV), (c) O 1s (530.0 and 531.6 eV), and (d) Ni 2p of the NT-1.

Table S3 The estimated percentage of surface OH group among the surface O in different composites, obtained from XPS.

Sample	OH content (%)
TiO ₂ nanotubes	21.8
NT-1	14.3
FNT-1	30.9

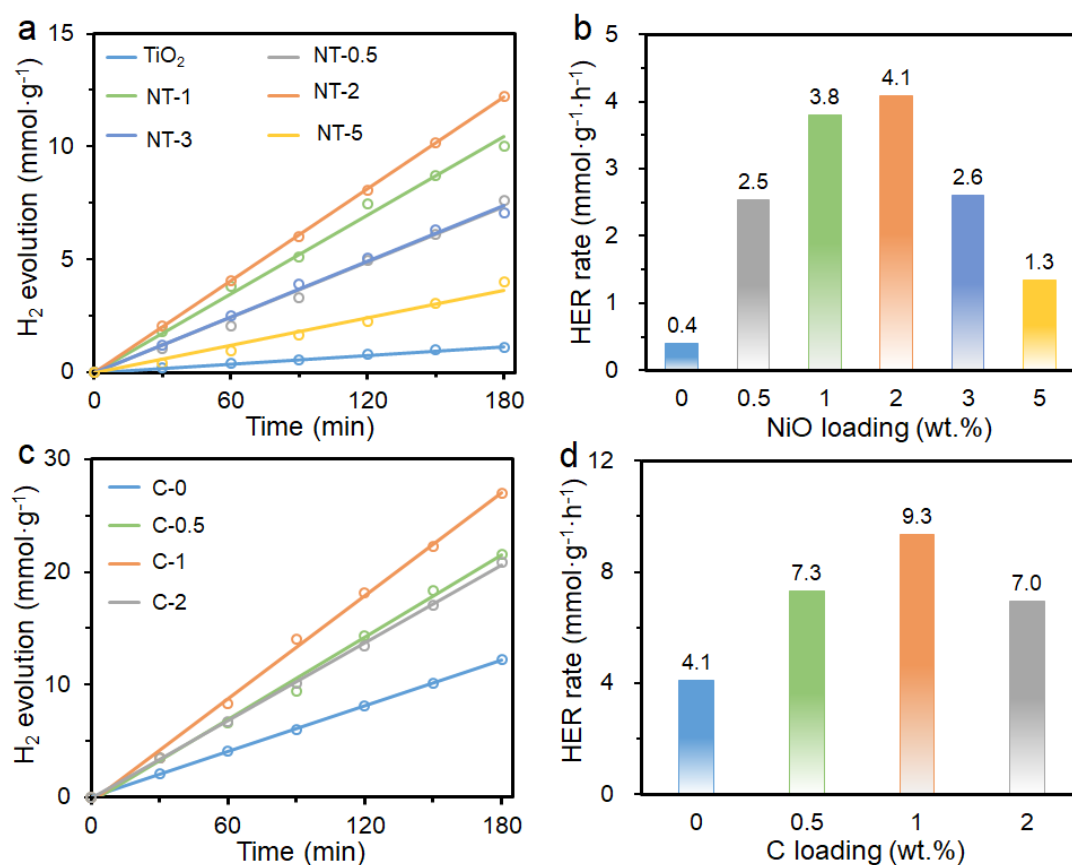


Fig. S9 (a) Hydrogen evolution and (b) HER rates of the TiO₂ nanotubes (TiO₂) and NT-x with varying nickel oxide loading (as labelled NT-0.5, NT-1, NT-2, NT-3 and NT-5), (c) Hydrogen evolution and (d) HER rates of CNT-y with varying carbon loading (as labelled CNT-0, CNT-0.5, CNT-1 and CNT-2).

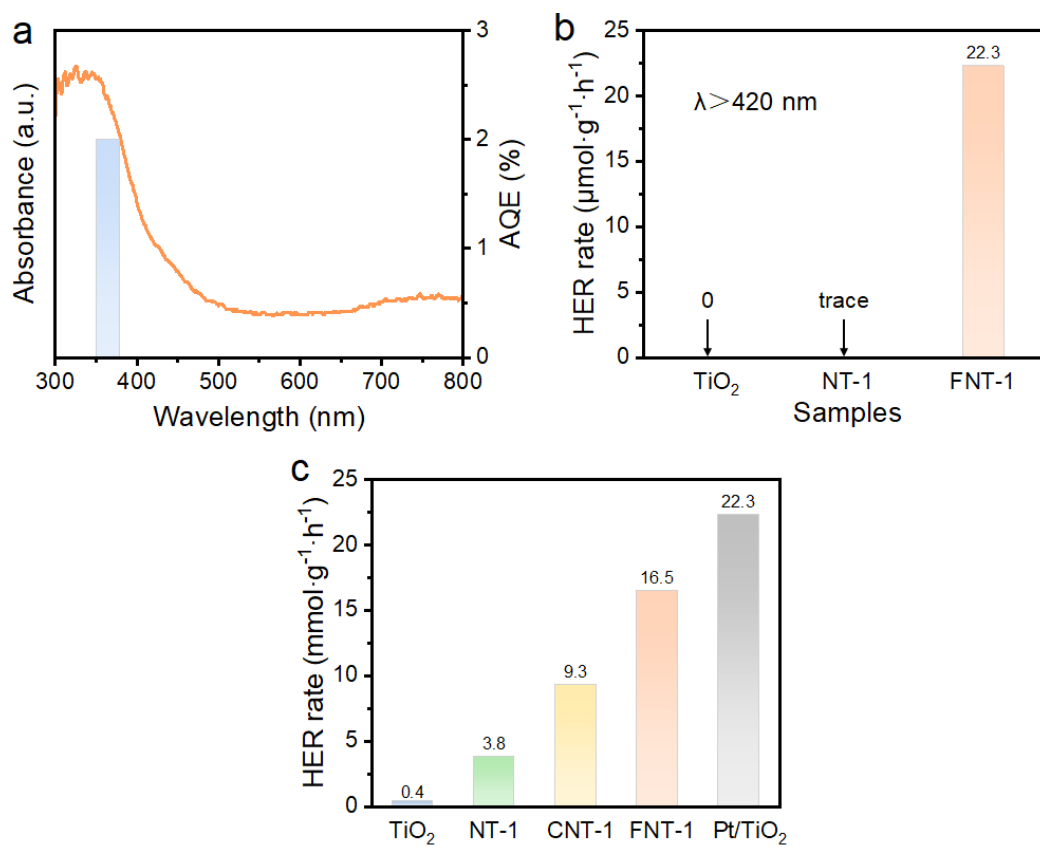


Fig. S10 (a) the UV-vis absorbance spectra and AQE at 365 nm for FNT-1, (b) HER efficiency of TiO₂, NT-1 and FNT-1 under visible light (>420 nm) irradiation. (c) HER rates for TiO₂ nanotubes (TiO₂), NT-1, CNT-1, FNT-1 and Pt/TiO₂.

Table S4 Comparison of photocatalytic activity in hydrogen production on recent TiO₂-based photocatalysts using transition metal cocatalyst.

Photocatalyst	Concentration (mg/mL)	Reactant solution	HER rate (mmol·g ⁻¹ ·h ⁻¹)	Incident light	Ref.
FNT-1	0.2	10 vol% methanol	16.5	300 W xenon lamp	This work
NiO-TiO _{2-x} /C	0.2	20 vol% methanol	1.6	300 W xenon lamp	12
Ni SA/TiO ₂	0.5	20 vol% methanol	2.9	280 W xenon lamp	13
a-NiSe _{1+x} /TiO ₂	0.2	25 vol% methanol	4.1	4 LED lights (365 nm, 3-W)	14
WSe _{2+x} /TiO ₂	0.625	25 vol% ethanol	3.8	4 LED lights (365 nm, 3 W)	15
Cu SA/TiO ₂	0.06	25 vol% methanol	16.6	100 mW/cm ² xenon lamp	16
Cu _x O/TiO ₂	0.2	20 vol% methanol	12.5	300 W xenon lamp	17
CuWO ₄ /TiO ₂	0.4	20 vol% TEOA	6.2	300 W xenon lamp	18
Co SA-TiO ₂	1	20 vol% methanol	1.7	300 W xenon lamp	19
Co ₃ O ₄ /TiO ₂	0.25	10 vol% TEOA	3.5	300 W xenon lamp	20
TiO ₂ /Au@MoS _{2+x}	0.625	25 vol% ethanol	7.9	4 LED lights (365 nm, 3 W)	21

a-NiSe_{1+x}: amorphous NiSe_{1+x} nanoclusters;

SA: single-atom;

TEOA: triethanolamine;

Vo: oxygen vacancy.

Table S5 Comparison of photocatalytic activity in hydrogen production on recent TiO₂-based composites with noble metal cocatalyst.

Photocatalyst	Concentration (mg/ml)	Reactant solution	HER rate (mmol·g ⁻¹ ·h ⁻¹)	Incident light	Ref.
Pt/TiO ₂	0.2	10 vol% methanol	24.6	300 W xenon lamp	22
Pt clusters/TiO ₂	0.2	50 % methanol	3.0	AM 1.5G	23
Pt-SA/TiO ₂	0.1	10 vol% methanol	25.56	300 W xenon lamp	24
Pt-SA/TiO ₂ -F	0.2	50 vol% methanol	13.7	365 nm LED (65 mW/cm ²)	25
Co-Pt DSA /TiO ₂	0.1	10 vol% methanol	43.47	300 W xenon lamp	24
Pd-TiO ₂	0.08	20 vol% methanol	24.6	300 W xenon lamp	26
Ag _x O/TiO ₂	0.2	10 vol% methanol	22.8	300 W xenon lamp	22
Au@N-TiO ₂	1	25 vol% methanol	4.9	300 W xenon lamp	27
Ru-SA/TiO ₂	0.2	20 vol% methanol	9.0	300 W xenon lamp	28
RuO _x /TiO ₂	0.5	10 vol% TEOA	13.4	300 W xenon lamp	29
Co-RuO _x /TiO ₂	0.5	10 vol% TEOA	38.4	300 W xenon lamp	29

SA: single-atom;
 DSA: dual single-atom.

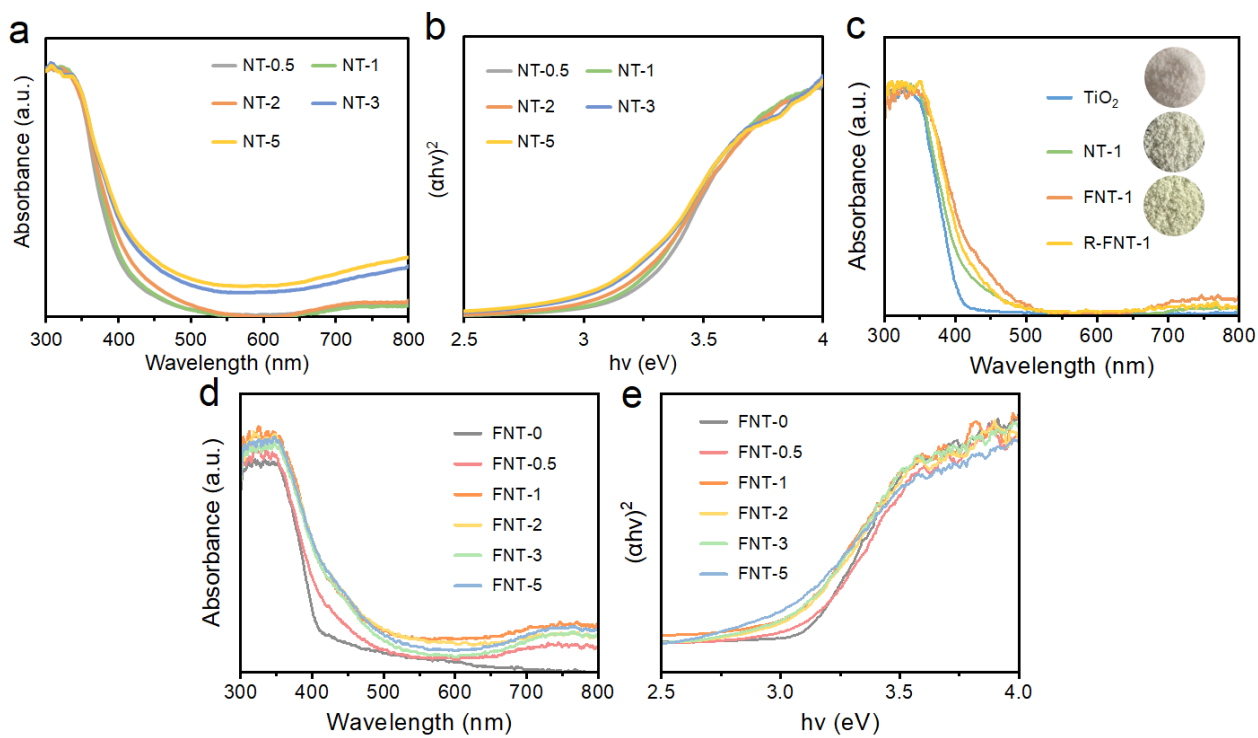


Fig. S11 (a) UV-vis absorption spectra and (b) corresponding Tauc plots of NT-x composites. (c) UV-vis absorption spectra of the TiO₂ nanotubes, NT-1, FNT-1 and R-FNT-1 (inset, optical images of the TiO₂ nanotubes, NT-1 and FNT-1). (d) UV-vis absorption spectra and (e) corresponding Tauc plots of FNT-x composites.

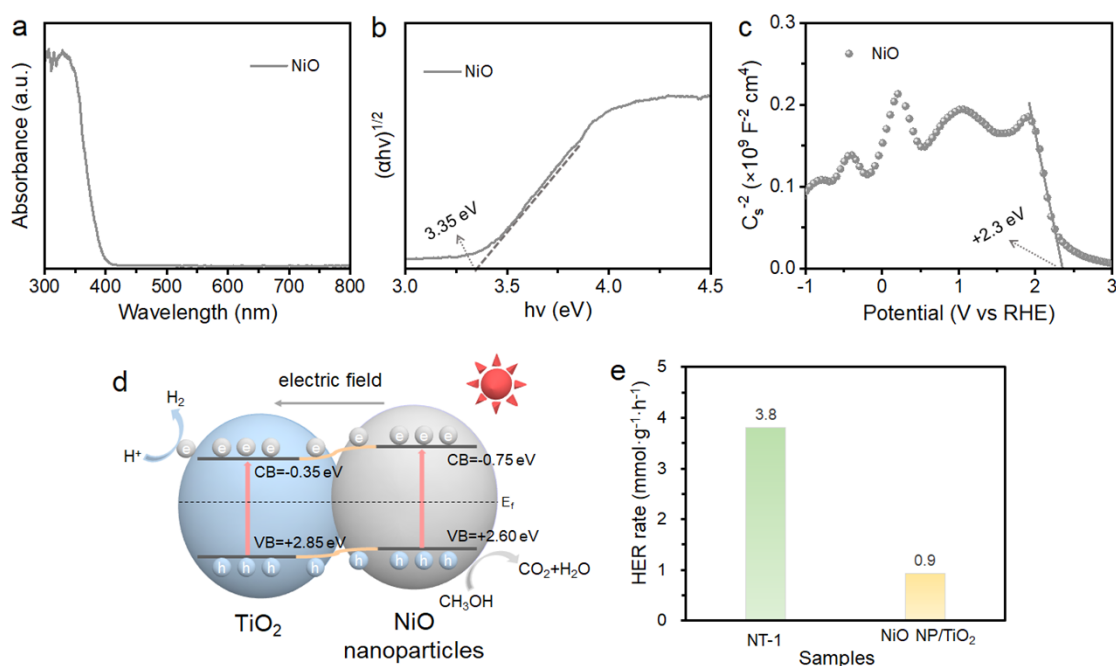


Fig. S12 (a) UV-vis absorption spectrum, (b) Tauc plot, and (c) Mott-Schottky plot of the control NiO NP; (d) schematic illustration of electron-hole separation on the control sample NiO NP/TiO₂ nanotubes under UV-vis light irradiation and (e) HER rates of NT-1 and the control sample NiO NP/TiO₂ nanotubes.

In general, the conduction-band edges (CB) of n-type semiconductor or valence-band edges (VB) of p-type semiconductor is more negative or positive of 0.1-0.3 eV than the flat-band potential. The present work uses 0.3 eV for demonstration, then the calculated CB of TiO₂ and VB of NiO are -0.35 eV and 2.60 eV vs. RHE (reversible hydrogen electrode), respectively.³⁰⁻³² According to the Tauc plots, the corresponding E_g of TiO₂ and NiO are 3.20 and 3.35 eV, respectively. The VB of TiO₂ and CB of NiO are therefore of 2.85 eV and -0.75 eV vs. RHE, respectively. Based on this, the schematic illustration of electron-hole separation on the control sample NiO NP/TiO₂ nanotubes under UV-vis light irradiation is shown in Fig. S12d.

References

- 1 G. Kresse and J. Hafner, *Phys. Rev. B*, 1993, **48**, 13115-13118.
- 2 G. Kresse and J. Hafner, *Phys. Rev. B*, 1994, **49**, 14251-14269.
- 3 J. P. Perdew, K. Burke and M. Ernzerhof, *Phys. Rev. Lett.*, 1996, **77**, 3865-3868.
- 4 A. Rohrbach, J. Hafner and G. Kresse, *Phys. Rev. B*, 2004, **69**, 075413.
- 5 Q. Xu, S. Cheah and Y. Zhao, *J. Chem. Phys.*, 2013, **139**, 024704.
- 6 D. Wang and X.-Q. Gong, *Nat. Commun.*, 2021, **12**, 158.
- 7 B. J. Morgan and G. W. Watson, *Surf. Sci.*, 2007, **601**, 5034-5041.
- 8 L. A. Burns, Á. V. Mayagoitia, B. G. Sumpter and C. D. Sherrill, *J. Chem. Phys.*, 2011, **134**, 084107.
- 9 S. Grimme, S. Ehrlich and L. Goerigk, *J. Comput. Chem.*, 2011, **32**, 1456-1465.
- 10 Y. Ide, N. Inami, H. Hattori, K. Saito, M. Sohmiya, N. Tsunoji, K. Komaguchi, T. Sano, Y. Bando, D. Golberg and Y. Sugahara, *Angew. Chem. Int. Ed.*, 2016, **55**, 3600-3605.
- 11 J. K. Nørskov, T. Bligaard, A. Logadottir, J. R. Kitchin, J. G. Chen, S. Pandelov and U. Stimming, *J. Electrochem. Soc.*, 2005, **152**, J23-J26.
- 12 X. Zhang, W. Xie, Z. Deng, G. Wang, A. Gao, H. Chen, B. Yang, Z. Wang, X. Su and C. Yang, *Colloids surf. A Physicochem. Eng. Aspects*, 2020, **587**, 124365.
- 13 S. Lv, M. Pei, Y. Liu, Z. Si, X. Wu, R. Ran, D. Weng and F. Kang, *Nano Res.*, 2022, **15**, 5848-5856.
- 14 D. Gao, X. Wu, P. Wang, H. Yu, B. Zhu and J. Yu, *Chem. Eng. J.*, 2021, **408**, 127230.
- 15 D. Gao, W. Zhong, X. Wang, F. Chen and H. Yu, *J. Mater. Chem. A*, 2022, **10**, 7989-7998.
- 16 B. H. Lee, S. Park, M. Kim, A. K. Sinha, S. C. Lee, E. Jung, W. J. Chang, K. S. Lee, J. H. Kim, S. P. Cho, H. Kim, K. T. Nam and T. Hyeon, *Nat. Mater.*, 2019, **18**, 620-626.
- 17 L. Cui, C. Niu, Y. S. Kang, R. A. Caruso and X. L. Zhang, *Nanoscale*, 2022, **14**, 17460-17465.
- 18 W. Wang, S. Mei, H. Jiang, L. Wang, H. Tang and Q. Liu, *Chin. J. Catal.*, 2023, **55**, 137-158.
- 19 X. Wu, S. Zuo, M. Qiu, Y. Li, Y. Zhang, P. An, J. Zhang, H. Zhang and J. Zhang, *Chem. Eng. J.*, 2021, **420**, 127681.
- 20 L. Wang, G. Tang, S. Liu, H. Dong, Q. Liu, J. Sun and H. Tang, *Chem. Eng. J.*, 2022, **428**, 131338.
- 21 D. Gao, P. Deng, J. Zhang, L. Zhang, X. Wang, H. Yu and J. Yu, *Angew. Chem. Int. Ed.*, 2023,

62, e202304559.

- 22 Y. Zhang, C. Niu, J. Liu, R. A. Caruso and X. L. Zhang, *J. Mater. Chem. A*, 2023, **11**, 25910-25917.
- 23 J. Cai, A. Cao, Z. Wang, S. Lu, Z. Jiang, X.-Y. Dong, X. Li and S.-Q. Zang, *J. Mater. Chem. A*, 2021, **9**, 13890-13897.
- 24 C. Wang, K. Wang, Y. Feng, C. Li, X. Zhou, L. Gan, Y. Feng, H. Zhou, B. Zhang, X. Qu, H. Li, J. Li, A. Li, Y. Sun, S. Zhang, G. Yang, Y. Guo, S. Yang, T. Zhou, F. Dong, K. Zheng, L. Wang, J. Huang, Z. Zhang and X. Han, *Adv. Mater.*, 2021, **33**, 2003327.
- 25 S. M. Wu, I. Hwang, B. Osuagwu, J. Will, Z. Wu, B. B. Sarma, F. F. Pu, L. Y. Wang, Z. Badura, G. Zoppellaro, E. Spiecker and P. Schmuki, *ACS Catal.*, 2023, **13**, 33-41.
- 26 Y. Zhou, H. Qin, S. Fang, Y. Wang, J. Li, G. Mele and C. Wang, *Catal. Sci. Technol.*, 2022, **12**, 7151-7160.
- 27 G. K. Naik, S. M. Majhi, K. U. Jeong, I. H. Lee and Y. T. Yu, *J. Alloys Compd.*, 2019, **771**, 505-512.
- 28 J. Li, D. Yi, F. Zhan, B. Zhou, D. Gao, D. Guo, S. Liu, X. Wang and J. Yao, *Appl. Catal. B Environ.*, 2020, **271**, 118925.
- 29 J. Shen, C. Luo, S. Qiao, Y. Chen, K. Fu, J. Xu, J. Pei, Y. Tang, X. Zhang, H. Tang, H. Zhang and C. Liu, *Adv. Funct. Mater.*, 2024, **34**, 2309056.
- 30 S. Meloni, G. Palermo, N. Ashari-Astani, M. Grätzel and U. Rothlisberger, *J. Mater. Chem. A*, 2016, **4**, 15997-16002.
- 31 J. W. Ondersma and T. W. Hamann, *Energy Environ. Sci.*, 2012, **5**, 9476.
- 32 K. Gelderman, L. Lee and S. W. Donne, *J. Chem. Educ.*, 2007, **84**, 685.